Strojniški vestnik - Journal of Mechanical Engineering 64(2018)no, 1-9
DOI:10.5545/sv-jme.2017.5084
Original Scientific Paper
Received for review: 2017-11-14
Received revised form: 2018-01-29
Accepted for publication: 2018-02-14

Design of an Apple-Picking End Effector

Yinggang Shi – Kaijia Zhu – Shenghang Zhai – Dewei Zhang – Li Liu* – Jizheng Zhao – Yan Long – Yongjie Cui
Northwest A&F University, College of Mechanical and Electronic Engineering, China

A motor-driven end effector with 9 degrees of freedom has been designed. Information of the joint position is transmitted to the potentiometer through gears to realize the position control for the finger joint. The maximum torque of the finger joint motor is verified by imposing a load on the end effector fingertip under the parabola-straight line angular velocity curve. The single-finger coordinate system and the whole-hand coordinate system are established for the end effector through the Denavit–Hartenberg (D-H) method. The forward kinematics and inverse kinematics analysis of the end effector are carried out. To realize the stationary motion of the end effector, the basic algorithms for the starting, stopping and accelerating of the finger joint is designed, based on the analysis of the grasping space using Monte Carlo method and the analysis of the angular displacement of motor using an isochronic interpolation algorithm. The control system is designed based on STM32F103RC to realize the stationary motion of the end effector. Using Tiny 6410, the remote wireless debugging system of the end effector is designed to realize independent control and remote wireless debugging of each joint motor.

Keywords: apple picking, end effector, trajectory planning, remote wireless debugging, STM32F103RC, Tiny6410

Highlights

- *A motor-driven end effector with 9 degrees of freedom is designed.*
- *The forward kinematics and inverse kinematics analysis of the end effector are carried out.*
- *This end effector can be independently controlled and debugged wirelessly.*
- *The mechanical strength of the end effector can meet the requirements of apple picking.*

0 INTRODUCTION

In China, apples are mostly harvested by human labour. Harvesting is expected to be automated as the farming population is gradually decreasing. He et al. [1] reported new variations of the shake-and-catch harvesting system in 2017. However, this method of picking frequently causes substantial fruit damage and the dropping of immature fruits. Researchers have proposed that the robotic system which mimics the human hand-picking process can improve manipulation performance and reduce damage [2]. However, one of the bottlenecks in the development of a robotic apple harvester is the lack of effectively functional apple picking end-effector to meet the challenging requirements for practical application, because the picking end-effector handle can plant materials directly and potentially influence the market value of the product [3].

The automatic picking of fruit requires higher-level mechanical control and feedback of the end effector [4]. At present, many experts and scholars have carried out related studies on the end effector which is used for picking round or oval fruits such as apple [5], tomato [6], orange [7], and kiwi [8]. To date, the end effector used for picking round or oval fruit has drive modes such as tendon transmission, belt drive, air pressure transmission, and hydraulic transmission. However, the end effector designed by adopting the abovementioned transmission modes has poor self-adaptability of grasping [9] and [10]. Bao et al. [11] designed a type of pneumatic flexible end-effector that can protect fruits from damage. Furthermore, the conventional off-line programming, force feedback check and other grasping posture debugging methods need to be operated by professionals, which is rather cumbersome. The flexible finger made of new materials has fairly strong adaptability and causes less damage to the fruit. However, the price is high, and the control system is rather complex. Therefore, it is imperative to design a cheaper debugging mode which allows farmers to independently set the end effector grasping posture to improve the grasping adaptability of the end effector. From the point of view of cost and efficiency, the design of such a debugging mode is conducive to the promotion of the round or oval fruit picking. Among apple, pear, peach, kiwi, and other round or oval fruits, a mature apple is representative in terms of weight and shape. Thus, this paper takes the apple picking as example for designing the end effector.

1 DESIGN OF THE OVERALL SYSTEM

In the process of apple picking, the end effector is required to envelop the fruit. The number of fingers is set as three. The three fingers are in a circular layout and are distributed evenly. Fig. 1 shows the design of

*Corr. Author's Address: College of Mechanical and Electronic Engineering, Northwest A&F University, NO. 3 Taicheng Road, Yangling 712100, Shaanxi, China, liuli_ren_79@nwsuaf.edu.cn

the overall layout of the end effector. A direct-current dynamo is used to drive the reduction gear to drive the finger, and the output shaft of the motor is connected with the potentiometer to realize the collection of the joint position information. Position-based control is used to ensure the dexterous operation of the end effector.

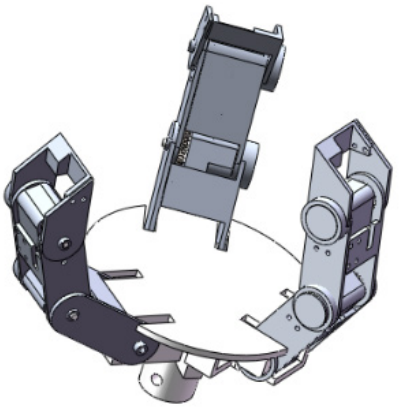

Fig. 1. *Overall layout of end effector*

The end effector has a total of nine degrees of freedom. The control system architecture of the end effector is shown in Fig. 2. The joint motor operation can be controlled after the input of the nine-channel PWM wave into the joint motor driver. To ensure that farmers can independently set the fruit grasping posture of the end effector, it is necessary to design a remote wireless debugging module to debug the grasping posture of the end effector. Meanwhile, the operation law for the starting, accelerating, and stopping of each joint motor is made into standard modules, which is stored in the memory of the lower computer controller. The lower computer carries out the joint trajectory planning according to the grasping posture of the end effector. Then, the joint trajectory of the end effector is constructed according to the results of trajectory planning and application of the modularized trajectory curve program of the starting, speeding, and stop of each joint motor and the even operation of the subroutine of the motor.

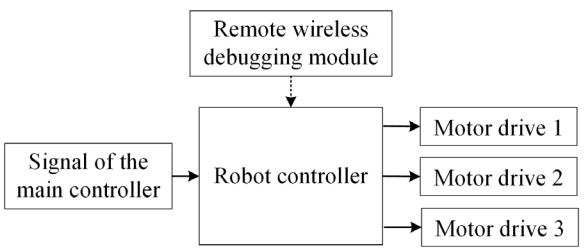

Fig. 2. *Architecture of the control system of the end effector*

2 DESIGN AND VERIFICATION OF MECHANICAL STRUCTURES OF END EFFECTOR

2.1 The Mechanical System Design

Mature apples are usually 80 mm to 100 mm in diameter. Each finger of the end effector is designed to consist of three knuckles whose lengths are 41 mm, 41 mm, and 30 mm. The mechanical structure of the single finger is shown in Fig. 3. At the end of the output shaft of the reduction motor, the rotating angle of the joint is transmitted to the potentiometer through the gear meshing, as shown in Fig. 4. GAM-N20 is selected as the joint deceleration motor, whose parameters are shown in Table 1. Fig. 5 shows the end effector made of polylactic acid (PLA) material through rapid prototyping technology.

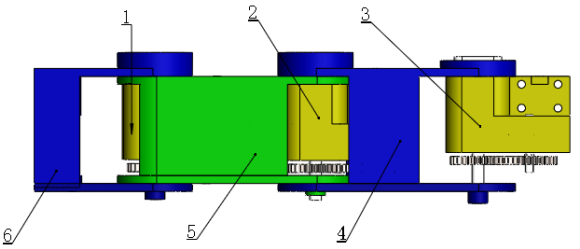

Fig. 3. *The mechanical structure of a single finger; 1) motor of far joint, 2) motor of middle joint, 3) motor of base joint, 4) base knuckle, 5) middle knuckle, and 6) fingertip*

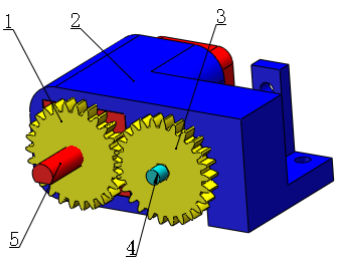

Fig. 4. *Detection mechanism of joint rotation angle; 1) output gear of the gearmotor, 2) motor housing, 3) potentiometer gear, 4) potentiometer shaft, and 5) gearmotor*

Table 1. *The parameters of the joint motor GAM-N20*

Rated voltage	6 V
No load speed	60 r/min
Load speed	48 r/min
Rated torque	0.098 Nm
Rated current	120 mA
Stopping torque	0.686 Nm
Stall current	200 mA
Reduction ratio	250

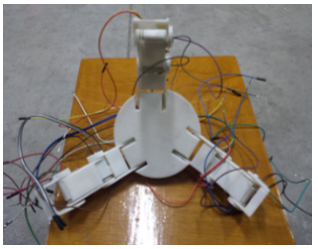

Fig. 5. *The 3D-printed end effector*

The weight of an apple is generally 180 g to 250 g. In the picking process, the distribution of the finger load is uniform without consideration of the reaction force of the fruit stem on the end effector. The load of each knuckle is shown in Eq. (1).

$$F = \frac{m \cdot g}{n} \cdot k, \tag{1}$$

where m is the weight of the apple, g is the acceleration of gravity, n is the number of the fingers and k is the safety factor. $n = 3$ represents the fact that the maximum load of the finger knuckle is to bear 1/3 of the weight of the apple. Considering an apple with a maximum mass of about 0.25 kg, the safety factor is set as 1.2, so the value of force is 0.98 N.

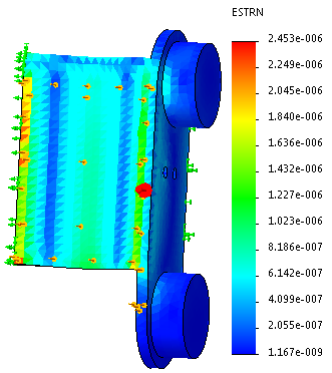

Fig. 6. *Stress distribution of middle finger knuckle*

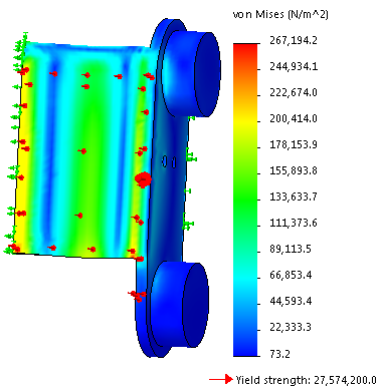

Fig. 7. *Strain distribution of middle finger knuckle*

In extreme cases, the fingertips bear all the weight of the fruits. Consider an apple with a maximum mass of about 0.25 kg. When distributed to each finger, the load is about 0.98 N as shown in Eq. (1). In the picking process, the middle finger bears the largest load. To simulate the mechanical strength of the finger, the load of 1 N is imposed on the tip of the middle finger with its basal joint fixed. The end effector is made of 1345 aluminium alloy, with a shear modulus of 27,000 MPa, a density of 2,700 kg/m^3, a yield strength of 27.574200 MPa, an elastic modulus of 69,000 MPa, and a Poisson's ratio of 0.33. The loading pattern, stress and strain stress of the middle finger are shown in Figs. 6 and 7, respectively. The simulation indicates that the minimum shear stress is 0.0000732 MPa and the maximum is 0.2671942 MPa; the minimum strain is 1.167×10^{-9}, and the maximum is 2.453×10^{-6}. The mechanical strength of the middle finger satisfies the requirement, as does the mechanical strength of other fingers [12].

2.2 Kinematic Analysis of End Effector

The single finger Denavit–Hartenberg (D-H) coordinate system of the end effector is established, as shown in Fig. 8. Its parameters are shown in Table 2.

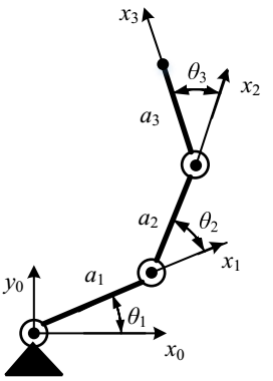

Fig. 8. *The single finger D-H coordinate system of the end effector*

Table 2. *Parameters of single finger D-H coordinate system of end effector*

link	θ_i [°]	d_i	a_i	α_i [°]	Variable range
1	θ_1	0	30	0	0 to 90
2	θ_2	0	41	0	0 to 90
3	θ_3	0	41	0	0 to 90

Set $s_x = \sin\theta_x$, $c_x = \cos\theta_x$, $s_{ijk} = \sin(\theta_i+\theta_j+\theta_k)$, $c_{ijk} = \cos(\theta_i+\theta_j+\theta_k)$, then the rotation matrix $\mathbf{A}_1$, $\mathbf{A}_2$, $\mathbf{A}_3$ can be obtained. Transformation matrix from

fingertip coordinate to base coordinate, as shown in Eq. (2) [13].

$$
\begin{aligned}
{}^{0}\mathbf{T}_3 &= \mathbf{A}_1 \times \mathbf{A}_2 \times \mathbf{A}_3 = \\
&= \begin{bmatrix} c_{123} & -s_{123} & 0 & a_1 c_1 + a_2 c_{12} + a_3 c_{123} \\ s_{123} & c_{123} & 0 & a_1 s_1 + a_2 s_{12} + a_3 s_{123} \\ 0 & 0 & 1 & 0 \\ 0 & 0 & 0 & 1 \end{bmatrix} = \\
&= \begin{bmatrix} n_x & o_x & a_x & p_x \\ n_y & o_y & a_y & p_y \\ n_z & o_z & a_z & p_z \\ 0 & 0 & 0 & 1 \end{bmatrix}.
\end{aligned} \tag{2}
$$

The inverse kinematics of the end effector is solved by using the algebraic method [14] and [15].

Eqs. (3) to (6) can be obtained by equation (2). Eqs. (7) and (8) can be obtained by substituting Eqs. (3) and (4) into Eqs. (5) and (6). Though Eqs. (7) and (8) θ_2 can be obtained, as shown in Eq. (9). Then, θ_1 can be solved by substituting Eq. (9) into Eq. (7), as shown in Eq. (10). Finally, θ_3 can obtained by Eqs. (3) and (4). The inverse kinematics equation of the finger of the end effector has many solutions, so it is necessary to consider the actual situation of picking and the requirement of the stability of motion.

$$c_{123} = n_x, \tag{3}$$

$$s_{123} = n_y, \tag{4}$$

$$a_1 c_1 + a_2 c_{12} + a_3 c_{123} = p_x, \tag{5}$$

$$a_1 s_1 + a_2 s_{12} + a_3 s_{123} = p_y, \tag{6}$$

$$a_1 c_1 + a_2 c_{12} = p_x - a_3 n_x, \tag{7}$$

$$a_1 s_1 + a_2 s_{12} = p_y - a_3 n_y, \tag{8}$$

$$\theta_2 = \arccos\left(\frac{\left(p_x - a_3 n_x\right)^2 + \left(p_y - a_3 n_y\right)^2 - a_1^2 - a_2^2}{2 a_1 a_2} \right), \tag{9}$$

$$\theta_1 = \arctan\left(\frac{p_y - a_3 n_y}{p_x - a_3 n_x}\right) - \arctan\left(\frac{a_2 \sin\theta_2}{a_1 + a_2 \cos\theta_2}\right), \tag{10}$$

$$\theta_3 = \arctan\left(\frac{n_y}{n_x}\right) - \theta_1 - \theta_2. \tag{11}$$

2.3 Trajectory Planning and Motor Checking

In the starting phase of the joint motor motion, the acceleration curve is set as a trapezoidal shape. The joint angular velocity of the end effector can be calculated by adopting the parabola-straight line velocity curve planning algorithm, so that the motion of the end effector can be stabilized [16] and [17]. Considering the mechanical structure of the end effector, each joint of the end effector is set to rotate from 0° to 90°. The maximum acceleration of joint motor is $\varepsilon_{max} = 5°/s^2$, and the maximum velocity is $w_{max} = 10°/s$. The speed of the motor of each joint is planned as shown in Eq. (12).

The angular velocity curve of each joint motor can be obtained by Eq. (12), as shown in Fig. 9.

$$
\omega(t) = \begin{cases}
\dfrac{\varepsilon_{max}}{2 \cdot t_1} \cdot t^2 & 0 < t \le t_1 \\
-\dfrac{1}{2} \cdot t_1 \cdot \varepsilon_{max} + t \cdot \varepsilon_{max} & t_1 < t \le t_2 \\
\varepsilon_{max} \cdot t_2 - \dfrac{1}{2} \cdot \dfrac{\varepsilon_{max}}{t_1} \cdot \left(t - t_1 - t_2\right)^2 & t_2 < t \le t_1 + t_2 \\
\varepsilon_{max} \cdot t_2 & t_1 + t_2 < t \le t_4 \\
\varepsilon_{max} \cdot t_2 - \dfrac{1}{2} \cdot \dfrac{\varepsilon_{max}}{t_1} \cdot (t - t_4)^2 & t_4 < t \le t_1 + t_4 \\
\varepsilon_{max} \cdot t_2 - \varepsilon_{max} \cdot \left(t - \dfrac{t_1}{2} - t_4\right) & t_1 + t_4 < t \le t_2 + t_4 \\
\dfrac{1}{2} \cdot \varepsilon_{max} \cdot \dfrac{\left(t - t_1 - t_2 - t_4\right)^2}{t_1} & t_2 + t_4 < t \le t_e
\end{cases} \tag{12}
$$

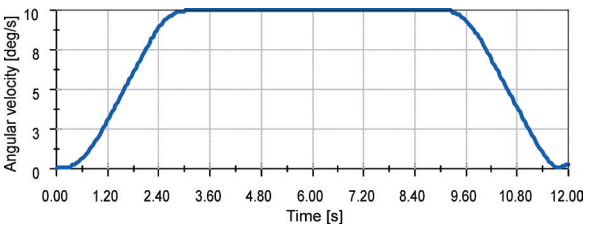

Fig. 9. *Angular velocity of the joint motor*

It can be seen from Fig. 13 that the velocity curve of the end effector becomes stable after trajectory planning. At the initial stage, the rate of change of velocity is a finite value. When the speed reaches the maximum value, it continues to run uniformly, then decelerates the speed. When reaching the endpoint, the joint angular velocity is 0. This can reduce the damage to the fruit. And it is also conducive to the operation of the motor.

Considering the finger weight of the end effector, the no-load checking of the motor is carried out by using SolidWorks software under the motion law shown in Fig. 9. The torque variation law of each joint motor is shown in Figs. 10 to 12. Motor torque 7, Motor torque 8, and Motor torque 9 represent the torque of Motor 7, Motor 8, and Motor 9, respectively.

The single finger movement of the end effector is simulated through applying the parabola-straight line speed curve planning algorithm. Results of the simulation show that the end effector runs smoothly.

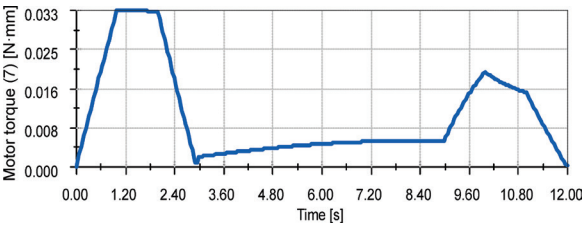

Fig. 10. *No-load torque diagram of base joint motor*

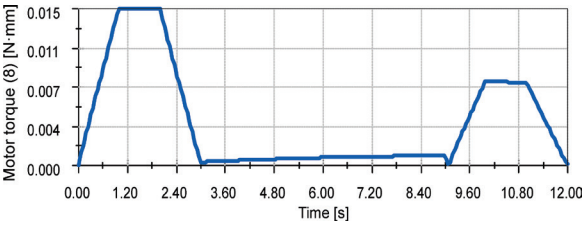

Fig. 11. *No-load torque diagram of middle joint motor*

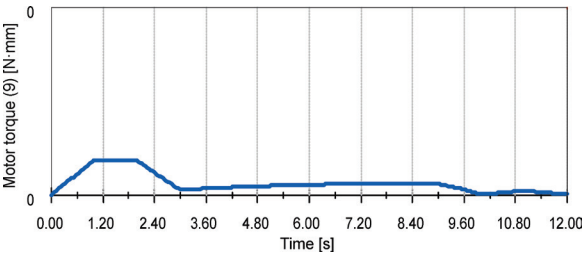

Fig. 12. *No-load torque diagram of distal joint motor*

2.4 Workspace Analysis of End Effector

The workspace of the end effector is solved by the Monte Carlo method [18] and [19]. The relationship between the fingertip of the end effector and the base coordinate is ${}^0T_3 = \mathbf{A}_1 \times \mathbf{A}_2 \times \mathbf{A}_3$. The motion space of the fingertip relative to the base coordinate refers to the motion space of the point at the location of (0,0,0), i.e. [20].

$$\begin{cases} p_{x1} = a_1 c_1 + a_2 c_{12} + a_3 c_{123} \\ P_{y1} = a_1 s_1 + a_2 s_{12} + a_3 s_{123} \end{cases}. \tag{13}$$

The rotation angle of each joint of the end effector is between 0° and 90°. When the rand function of MATLAB software is applied, 80,000 points in the range of the angle are generated and substitute them into Eq. (13). The workspace of the fingertip is calculated by using the scatter function, as shown in Fig. 13. In the same way, the sports space of the middle and distal finger knuckles of the single finger in the base coordinate is shown in Eqs. (14) and (15).

Combining with the mechanical mechanism of the end effector, the whole hand coordinate system is established by using the D-H method, as shown in Fig. 14. From the mechanical structure of the end effector, the D-H coordinate system parameters are learned and are shown in Table 3.

$$\begin{cases} p_{x1} = a_1 c_1 \\ P_{y1} = a_1 s_1 \end{cases}, \tag{14}$$

$$\begin{cases} p_{x2} = a_1 c_1 + a_2 c_{12} \\ P_{y2} = a_1 s_1 + a_2 s_{12} \end{cases}. \tag{15}$$

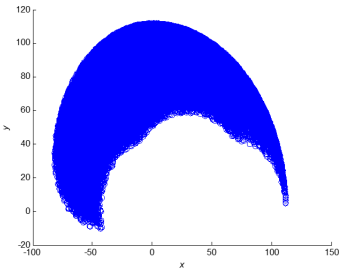

Fig. 13. *Fingertip workspace*

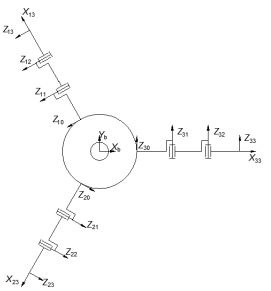

Fig. 14. *Whole-hand D-H coordinate system*

Table 3. *D-H parameters of finger base coordinate to palm base coordinate*

Parameter	d	θ [°]	α [°]	a
Z_{01}	0	–120	90	42.22
Z_{02}	0	0	90	42.22
Z_{03}	0	120	90	42.22

The transformation matrix of the Z_{01} coordinate system relative to the Z_0 coordinate system is shown in Eq. (16) [20].

$$\mathbf{A}_{01} = \begin{bmatrix} c_{01} & -s_{01}\cos\alpha_{01} & s_{01}\sin\alpha_{01} & a_{01}c_{01} \\ s_{01} & c_{01}\cos\alpha_{01} & -c_{01}\sin\alpha_{01} & a_{01}s_{01} \\ 0 & \sin\alpha_{01} & \cos\alpha_{01} & d_{01} \\ 0 & 0 & 0 & 1 \end{bmatrix}. \tag{16}$$

The transformation relationship between finger 1 of the end effector and the base coordinate is ${}^{b}T_{13}=\mathbf{A}_{01}\times\mathbf{A}_{1}\times\mathbf{A}_{2}\times\mathbf{A}_{3}$. The motion space of the fingertip of finger 1 relative to the base coordinate refers to the motion space of the point at the location of (0,0,0) , as shown in Eq. (17).

$$\begin{aligned} p_x &= c_{01}\left(a_1 c_1 + a_2 c_{12} + a_3 c_{123} + a_{01} + a_{01}\right), \\ p_y &= s_{01}\left(a_1 c_1 + a_2 c_{12} + a_3 c_{123} + a_{01} + a_{01}\right), \\ p_z &= \sin\alpha_{01}(a_1 s_1 + a_2 s_{12} + a_3 s_{123}). \end{aligned} \tag{17}$$

Based on Eq. (11), the workspace of the fingertip of finger 1 relative to the base coordinate of the hand can be calculated, as shown in Fig. 15.

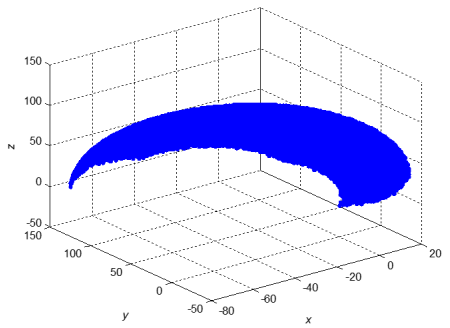

Fig. 15. *Fingertip workspace of finger 1*

In the same way, the images of the fingertips of finger 2 and finger 3 relative to the palm base coordinate can be calculated. The shape is the same as that in Fig. 15, but the images have different positions in the workspace. Using the fingertips of three fingers, the point of workspace can be obtained with the position equation of palm base coordinates. Using the cat function of MATLAB software, X coordinate, Y coordinate, and Z coordinate of the fingertip are combined. Then the whole workspace can be obtained by using the scatter3 function. Fig. 16 shows that the three fingertips can form a better envelope for the fruit from the whole-hand working space.

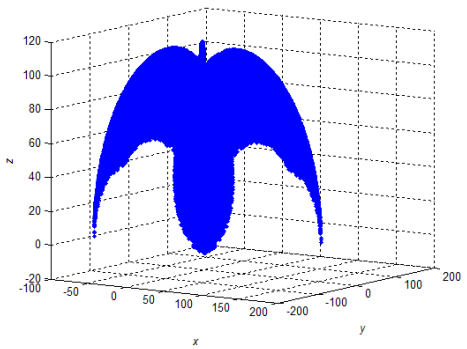

Fig. 16. *The workspace of the whole hand*

3 DESIGN OF CONTROL SYSTEM

3.1 Design of Remote Wireless Debugging Software

STM32F103RC is selected as the controller of the end effector. According to the overall system design requirements, the grasping posture of the end effector shall be adjusted by the remote wireless debugging module and downloaded to the controller storage. Meanwhile, the well-designed motor rotation trajectory curve shall also be stored in the Memory of the controller. The controller parses the control command conveyed by the main controller of the picking robot [21] and [22], and then retrieves different grasping gestures of the end effector and corresponding planned trajectory curve of the joint motor to drive the joint motor, thus realizing the grasping gesture of the end effector. Chip YT5188 is selected to collect the information of the rotation angle by checking the output end of the potentiometer at the corner of motors, which constitutes the motor position feedback control system. NRF24L01 is adopted as the wireless transmission model, which can realize point-to-point transmission. It communicates with the controller via SPI port. It can send or accept as many as 32 bytes at a time after configuration.

The control mode of the end effector controller includes an operation mode, a debugging mode, a download-the-initial-address mode, and a download-the-final-address mode.

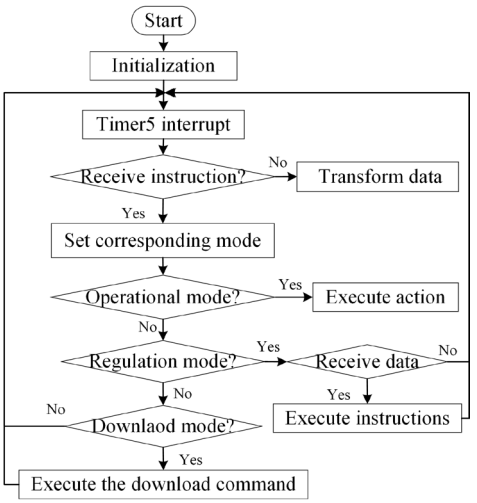

Fig. 17. *Software procedure of the end effector controller*

The software procedure of the end effector controller is shown in Fig. 17. The main program has been testing the mode zone bit. When the different mode zone bits are in place, the controller runs in

Table 4. *Relationship between the motor performance period, displacement and pulse increment*

	Acceleration (A)		Uniform acceleration (UA)					Variable deceleration (VB)				
Time [s]	$5t/8$	t	$t/5$	$2t/5$	$3t/5$	$4t/5$	t	$t/5$	$2t/5$	$3t/5$	$4t/5$	t
Displacement increment [deg]	0.20	0.63	0.60	0.80	1.00	1.20	1.40	1.59	1.75	1.87	1.95	1.99
Pulse increment	1	4	3	4	5	6	7	8	9	10	10	10

corresponding mode. Following a cycle of 50 ms, the timer interrupt 5 tests whether the data of remote wireless debugging module have been received. When the data are received, it will determine whether it is a command or operation data. If it is a command, a corresponding zone bit will be put in place. If it is operation data, it will be transformed and saved into the global variable, waiting for the function reference.

Table 5. *Integral displacement planning and design*

Displacement S (angle) [deg]	Planning algorithm
$0 < S \leq 0.83$	Run to the destination address
$0.83 < S \leq 6.66$	Start acceleration planning
$6.66 < S \leq 15.83$	Start acceleration planning and uniform acceleration planning
$15.83 < S \leq 25$	Start acceleration planning, uniform acceleration planning and variable deceleration planning
$25 < S \leq 30.8$	Start acceleration planning, uniform acceleration planning, variable deceleration planning and variable deceleration planning while decelerating.
$30.8 < S \leq 31.65$	Start acceleration planning, uniform acceleration planning, variable deceleration planning, variable deceleration planning while decelerating and variable planning while decelerating.
$31.65 < S$	Start phase planning, uniform velocity planning, deceleration planning

According to the motor control requirement, the pulse is required to be 1 ms to 2 ms. The clock frequency of the timer is set as 1 MHz and the cycling period is 20 ms, and then the timer duty cycle corresponding to 1 ms to 2 ms is 1,000 to 2,000. The motor rotation angle is 180 degrees, so the control accuracy of the controller is 0.18 degree. It can be seen from Eq. (12) that the motor rotates 0.83 degree at the beginning and accelerating period, rotates 5 degrees at the uniformly accelerating period and rotates 9.1667 degree at the decelerating phase. The interpolation method is designed based on the control accuracy of the motor. 2 points are interpolated at the acceleration stage, i.e. $5t/8$ and t ($t \leq 1$ s). At the uniformly accelerating period (1 s $< t \leq 2$ s), five points are interpolated isochronally. At the decelerating phase (2 s $< t \leq 3$ s), five points are interpolated isochronally. The interpolation point satisfying the abovementioned requests can be figured out based on the requirement of motor control, which is shown in Table 4.

The control law at the decelerating phase and the initialization phase is just on the contrary. At the uniform motion stage, the isochronal interpolation method is adopted. The interpolation point is proportional to the time of the uniform motion. There is an interpolation every 40 ms, and the pulse increment is 2. Based on the abovementioned control algorithm, finally, the motor displacement planning algorithm is designed, which is shown in Table 5. The motor operation process is designed based on the motor control law in Table 5.

3.2 Design of Remote Wireless Debugging Software

For the sake of convenient and simple control of the end effector, remote wireless debugging software was designed based on Tiny6410. The development environment was established adopting Linux operation system and Qt software.

The system invokes the driving procedure using Linux, operates input/output (I/0) interface and reads the command on the touch screen of Tiny 6410. The posture debug data of the end effector is sent to the transformation module via the serial port which will send the control command and data to the manipulator controller STM32F103RCT6 through the wireless communication module NRF24L01.

According to the above requirements, the software procedure of the remote wireless debugging module is designed, as shown in Fig. 18. The software interface is shown in Fig. 19. After the debugging software starts, the mode shall be selected first. When the operation mode is selected, other three modes shall be hidden. When the debugging mode is selected, the operation mode is hidden. Only under the debugging mode can the initial address and simulation address be downloaded. Control the location of the joint motor of the end effector with a slider control. When the slider slides, corresponding private slots will call a serial port to write the function. The debugging data will be

sent to the controller of the end effector through the serial port.

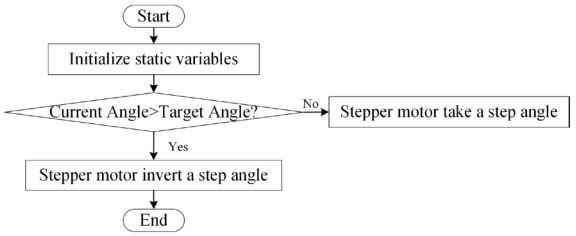

Fig. 18. *Software procedure of remote wireless debugging module*

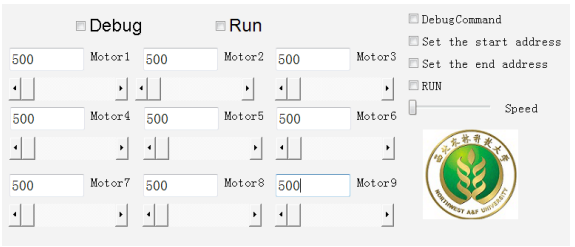

Fig. 19. *Software interface*

After the software runs, if the running mode or debugging mode is not selected, check the command check box or slide the slider, and the data will not be sent out. When the operation mode is chosen, the debugging mode, debugging order sending, the initial address downloading, and the final address downloading will be hidden. When the debugging mode is chosen, the operation mode and operation command will both be hidden, and the check boxes of sending debugging command, downloading initial command and downloading terminal command can be switched arbitrarily.

4 EXPERIMENTS AND RESULTS

To verify the performance of end effector, design an experiment as follows. Three fresh market apple varieties were chosen for this study. These varieties were Shaanxi Luo Chuan (Type 1) and Hong Xing (Type 2) and Fuji (Type 3). The end-effector conducts tests for 60 times (60 fruits), and 20 apples were selected for each variety. Before the experiment, ensure that the surface of the apple is intact so that it can be compared with the surface of the apple after the experiment to see if the force is appropriate. Then, take the apple and change the angle that the manipulator grasps from 0° to 180° to see if the end effector can grasp the apple firmly.

The results of the experiment are shown in Table 5. Type 1 and Type 2 apples could be grasped without dropping successfully. But the maximum of Type 3 apple failed to be grasped during the experiment. In the experiments with different gripping angles, apples were grasped without dropping except the maximum of Type 3, as shown in Fig. 20. After experiments, there was no obvious damage caused by the grasping experiment on the apple surface. The results show that the grasping force of the picking manipulator meets the requirement.

Table 6. *The results of the experiment*

Variety	Minimum mass [kg]	Maximum mass [kg]	Average mass [kg]	Success ratio [%]
Type 1	0.1803	0.2478	0.2369	100
Type 2	0.1803	0.2478	0.1992	100
Type 3	0.1779	0.3420	0.2361	95

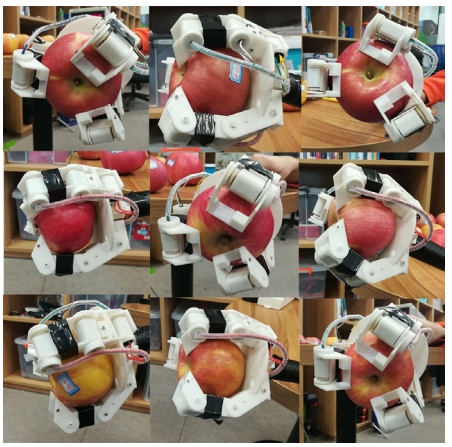

Fig. 20. *Experiment of grasping apple*

5 CONCLUSIONS

This paper presented the design of an end effector for apple picking with 9 degrees of freedom adopting the direct-current (DC) motor directly driven joints. The device can produce a grasp similar to the human hand-picking process by precise control of the joint motor, greatly improving the quality and efficiency of the picking. The experiment indicates that the end effector can successfully grab an apple with a mass between 0.18 kg and 0.25 kg and the force of the picking manipulator meet the requirement. The position control system is established based on information of the joint position transmitted to the potentiometer through gears. The velocity curve of the end effector becomes stable after trajectory planning. According to the analysis of the grasping space using the Monte Carlo method and the analysis of the angular displacement of motor using an isochronic interpolation algorithm, the end effector controller and remote wireless debugging module are designed,

which enables the farm workers to independently debug the grasping postures of the end effector and improves the grasping adaptiveness of the end effector. Other benefits of the design include its low cost and relatively simple design. Future research needs to be focused on the precise control of grasping force of the end effector to effectively prevent fruits from being damaged.

6 ACKNOWLEDGEMENTS

This research is supported by science and technology innovation projects of Shaanxi Province in China (No. 2015KTCQ02-12); Students' Innovative Research Plan of Northwest A&F University (No. 1201710712053); The authors also gratefully acknowledge the helpful comments and suggestions of the reviewers, which have improved the presentation.

7 REFERENCES

[1] He, L., Fu, H., Sun, D., Karkee, M., Zhang, Q. (2017). Shake-and-catch harvesting for fresh market apples in trellis-trained trees. *Transactions of the ASABE*, vol. 60, no. 2, p. 353-360, **DOI:10.13031/trans.12067**.

[2] Davidson, J., Silwal, A., Karkee, M. Mo, C., Zhang, Q. (2016). Hand-picking dynamic analysis for undersensed robotic apple harvesting. *Transactions of the ASABE*, vol. 57, no. 4, p. 745-758, **DOI:10.13031/trans.59.11669**.

[3] Monta, M., Kondo, N., Ting, K.C. (1998). End-effectors for tomato harvesting robot. *Artificial Intelligence Review*, vol. 12, no. 1-3, p. 11-25, **DOI:10.1023/A:1006595416751**.

[4] Zhao, D.A., Lv, J., Ji, W., Zhang, Y., Chen, Y. (2011). Design and control of an apple harvesting robot. *Biosystems Engineering*, vol. 110, no. 2, p. 112-122, **DOI:10.1016/j.biosystemseng.2011.07.005**.

[5] Kataoka, T., Hiroma, T., Ota, Y. (1998). Development of a harvesting hand for apples. *Advanced Robotics*, vol. 13 . no. 3, p. 293-294, **DOI:10.1163/156855399X00612**.

[6] Wang, G.H., Yu, Y.B., Feng, Q.C. (2016). Design of end-effector for tomato robotic harvesting. *IFAC-PapersOnLine*, vol. 49, no. 16, p. 190-193, **DOI:10.1016/j.ifacol.2016.10.035**.

[7] Flood, S.J., Burks, T.F., Teixeira, A.A. (2006). Physical properties of oranges in response to applied gripping forces for robotic harvesting. *Transactions of the ASABE*, vol. 49, no. 2, p. 341-346, **DOI:10.13031/2013.20635**.

[8] Chen, J., Wang, Hu., Jiang, HR., Gao, H., Lei, WL., Dang, GR.(2012). Design of end-effector for kiwifruit harvesting robot. *Transactions of the Chinese Society of Agricultural Machinery*, vol. 43, no. 10, p. 151-154, 199, **DOI:10.6041/j.issn.1000-1298.2012.10.027**. (in Chineese)

[9] Li, G.L., Ji, C.Y., Gu, B.X., Xu, W.Y., Dong, M. (2016) Kinematics analysis and experiment of apple harvesting robot manipulator with multiple end-effectors. *Transactions of the Chinese Society for Agricultural Machinery*, vol. 47, no. 12, p. 14-21, **DOI:10.6041/j.issn.1000-1298.2016.12.003**.

[10] Carreon, A., Baltazar, A., Kim, J.-Y. (2015). Determination of contact evolution on a soft hemispherical probe using ultrasound. *IEEE Sensors Journal*, vol. 15, no. 9, p. 5303-5311, **DOI:10.1109/JSEN.2015.2439293**.

[11] Bao, G.J., Gao, F., Xun, Y., Du, M.Y., Yang, Q.H.(2009). Flexible end-effector based on flexible pneumatic actuator and its grasping model. *Transactions of the Chinese Society of Agricultural Engineering*, vol. 25, no. 10, p 121-126, **DOI:10.3969/j.issn.1002-6819.2009.10.022**.

[12] Shi, Y.G., Guo, Y., Liu, L., Zhao, J.Z., Chen, J., Cui, Y.J.(2015). Design of an end effector for crawling roundlike fruits. *Academic Journal of Manufacturing Engineering*, vol. 14, no. 1, p. 46-54.

[13] Cheng, G., Xu, P., Yang, D.-H., Li, H., Liu, H.-G. (2013). Analysing kinematics of a novel 3CPS parallel manipulator based on rodrigues parameters. *Strojniški vestnik - Journal of Mechanical Engineering*, vol. 59, no. 5, p. 291-300, **DOI:10.5545/sv-jme.2012.727**.

[14] Wang, H.S., Zhan, D.Y., Huang, P.L., Chen, W.F. (2015). Inverse kinematics of a heavy duty manipulator with 6-DOF based on dual quaternion. *Journal of Central South University*, vol. 22, no. 7, p. 2568-2577, **DOI:10.1007/s11771-015-2786-1**.

[15] Chiang, M.H., Lin, H.T. (2011). Development of a 3D parallel mechanism robot arm with three vertical-axial pneumatic actuators combined with a stereo vision system. *Sensors*, vol. 11, no. 12, p. 11476-11494, **DOI:10.3390/s111211476**.

[16] Shi, Y.G., Guo, Y., Liu, L., Zhao, J.Z., Chen, J., Cui, Y.J. (2016). Analysis on the workspace of the picking manipulator for round fruits. *Revista de la Facultad de Ingeniería*, vol. 31, no. 4, p. 272-284, **DOI:10.21311/002.31.4.24**.

[17] Boryga, M. (2014). Trajectory planning of an end-effector for path with loop. *Strojniški vestnik - Journal of Mechanical Engineering*, vol. 60, no. 12, p. 804-814, **DOI:10.5545/sv-jme.2014.1965**.

[18] Chaudhury, A.N., Ghosal, A. (2017). Optimum design of multi-degree-of-freedom closed-loop mechanisms and parallel manipulators for a prescribed workspace using Monte Carlo method. *Mechanism and Machine Theory*, vol. 118, p. 115-138, **DOI:10.1016/j.mechmachtheory.2017.07.021**.

[19] Lee, P.C., Lee, J.J. (2016). On the kinematics of a new parallel mechanism with Schoenflies motion. *Robotica*, vol. 34, no. 9, p. 2056-2070, **DOI:10.1017/S0263574714002732**.

[20] Dupac, M., Noroozi, S. (2014). Dynamic modeling and simulation of a rotating single link flexible robotic manipulator subject to quick stops. *Strojniški vestnik - Journal of Mechanical Engineering*, vol. 60, no. 7-8, p. 475-482, **DOI:10.5545/sv-jme.2013.1544**.

[21] Cheng H.Y., Hu Z.Y., Chen W.Y. (2015). The flow control method of foamed bitumen. *International Journal of Heat and Technology*, vol. 33, no. 3, p. 145-150, **DOI:10.18280/ijht.330322**.

[22] Kesavan E., Gowthaman N., Tharani S., Manoharan S., Arunkumar E. (2016). Design and implementation of internal model control and particle swarm optimization based PID for heat exchanger system. *International Journal of Heat and Technology*, vol. 34, no. 3, p. 386-390, **DOI:10.18280/ijht.340306**.